HHS Public Access

Author manuscript

AJR Am J Roentgenol. Author manuscript; available in PMC 2016 December 12.

Published in final edited form as:

AJR Am J Roentgenol. 2015 April ; 204(4): W439–W448. doi:10.2214/AJR.14.13373.

Dynamic Contrast-Enhanced MRI for the Detection of Prostate Cancer: Meta-Analysis

Cher Heng Tan[1], **Brian Paul Hobbs**[2], **Wei Wei**[2], and **Vikas Kundra**[3,4]

[1]Department of Diagnostic Radiology, Tan Tock Seng Hospital, 11 Jalan Tan Tock Seng, Singapore 308433

[2]Department of Biostatistics, The University of Texas M. D. Anderson Cancer Center, Houston, TX

[3]Department of Diagnostic Radiology, The University of Texas M. D. Anderson Cancer Center, Houston, TX

[4]Department of Cancer Systems Imaging, The University of Texas M. D. Anderson Cancer Center, Houston, TX

Abstract

Objective—The purpose of this study was to systematically review and meta-analyze dynamic contrast-enhanced MRI (DCE-MRI) for the detection of prostate cancer in comparison with standard evaluation with T2-weighted imaging.

Materials and Methods—A PubMed electronic database search for the terms “dynamic contrast-enhanced,” “prostate,” and “MRI” was completed for articles up to September 17, 2013. All included studies had histopathologic correlation. Two by two contingency data were constructed for each study. A binormal bayesian ROC model was used to estimate and compare sensitivity, specificity, and AUC among eligible modalities.

Results—Both DCE-MRI (0.82–0.86) and diffusion-weighted MRI (DWI) (0.84–0.88) yielded significantly better AUC than T2-weighted imaging (0.68–0.77). Moreover, partial AUC for the combination of DCE-MRI, DWI, and T2-weighted imaging was improved significantly (0.111; 0.103–0.119) when compared with DCE-MRI alone (0.079; 0.072–0.085) and T2-weighted imaging alone (0.079; 0.074–0.084) but not DWI alone (0.099; 0.091–0.108). Sensitivity and specificity were similar among the four modalities.

Conclusion—DCE-MRI improves AUC of tumor detection overall compared with T2-weighted imaging alone. Methods for DCE-MRI analysis require standardization, but visual analysis performs similar to semiquantitative methods. A two-parameter approach using DCE-MRI and T2-weighted imaging or DWI and T2-weighted imaging may be sufficient, and the latter may be more favorable for most routine prostate cancer imaging.

Keywords

cancer; dynamic contrast-enhanced MRI (DCE-MRI); MRI; prostate

Address correspondence to C. H. Tan (tchers1977@gmail.com).

Conventional MRI evaluation of the prostate gland for prostate cancer hinges on high-resolution T2-weighted spin-echo imaging. The normal peripheral zone (PZ) of the prostate gland shows hyperintensity approaching water because of the presence of fluid contained within the acinar glands. Tumor is hypointense. Benign prostatic hyperplasia (BPH), prostatitis, and postbiopsy hemorrhage are well-known entities that confound the diagnosis of prostate cancer on T2-weighted imaging because of similarities in signal intensity and morphologic characteristics [1].

According to a meta-analysis by Sonnad et al. [2], MRI using T2-weighted imaging alone fares poorly in making the diagnosis of prostate cancer, with a maximum joint sensitivity and specificity rate of 74%. The meta-analysis by Engelbrecht et al. [3], with a published joint sensitivity and specificity rate of 71%, corroborated the earlier findings by Sonnad et al. There is a need for better imaging to improve diagnosis.

Dynamic contrast-enhanced MRI (DCE-MRI) has been increasingly applied to prostate imaging in large centers. It is usually included as part of multiparametric MRI for locating tumor foci. At present, multiparametric MRI is considered to be composed of two, three, or all of the following: T2-weighted imaging assessing hydration status, diffusion-weighted MRI (DWI) assessing restriction of random molecular motion, MR spectroscopy (MRS) assessing the concentration of metabolites (in prostate cancer, this most commonly refers to the ratio between choline and creatine vs citrate), and DCE-MRI assessing vascular properties [4].

In recent years, it has been suggested that multiparametric MRI that includes DCE-MRI, can improve the discrimination of malignant from benign prostatic tissues [5, 6]. This is significant for localizing the tumor in the prostate and is increasingly expected to help guide therapy. There are also recent data suggesting that multiparametric MRI may have a role in active surveillance of low-risk patients [7].

Multiparametric MRI, by virtue of its ability to discriminate tissues on the basis of function, adds value to conventional MRI that focuses on anatomic delineation. However, among the multiparametric techniques, the contribution of DCE-MRI is not clear. A number of studies have suggested added value of DCE-MRI for diagnosing prostate cancer. The aim of our study was to systematically review and meta-analyze this technique for the detection of prostate cancer in comparison with standard evaluation with T2-weighted imaging.

Materials and Methods

Literature Search

A literature search was performed according to the Preferred Reporting Items for Systematic reviews and Meta-Analyses guidelines [8, 9]. A comprehensive systematic literature review was completed for articles up to September 17, 2013. The PubMed and Embase electronic databases were searched. The literature search was limited to English language publications and human subjects. The following medical subject headings terms and keywords were used in the search: “dynamic contrast-enhanced,” “prostate,” and “MRI.” The abstracts of all relevant articles available on the database before September 17, 2013, were reviewed.

The study design inclusion criteria were broad and included retrospective and prospective studies. Articles were excluded if they were editorials, commentaries, or case reports. Specific inclusion criteria for articles were as follows: patients with histologically proven prostate cancer; diagnostic tests included DCE-MRI with or without other methods of imaging, such as T2-weighted imaging, MRS, and DWI; reference standard was histologic diagnosis; and sufficient data were reported to enable construction of two by two contingency tables. Only articles that used histopathologic results to directly reference independently derived DCE-MRI findings were considered for analysis. Those in which the DCE-MRI findings were retrospectively measured using prefabricated ROI maps derived from either histopathology or T2-weighted imaging were excluded to avoid potential bias.

Data Extraction

When we used the above-mentioned search terms, the abstracts of a total of 335 articles from PubMed were retrieved. Of these, 279 articles were initially excluded: 75 review articles, 65 technical reports (software, computer-assisted detection, DCE-MRI methodology, reporting, technologic assessment), 42 studies evaluating MRI for treatment response assessment, 23 studies that retrospectively evaluated DCE-MRI using prefabricated ROI maps, 21 non-English-language articles (but with English language abstracts), 22 ex-vivo or animal studies, 12 biopsy-related studies, seven studies that did not include DCE-MRI as a method or did not test for diagnostic performance of DCE-MRI, six studies with nonprostate cancer or noncancer subjects, and five case reports or editorial notes.

Full text evaluation of the remaining 56 articles was performed. Among these, 32 had to be excluded for the following reasons: one review article, one article that included patients reported in another listed article, two that did not include DCE-MRI as a method, three technical reports, eight studies that retrospectively evaluated DCE-MRI using prefabricated ROI maps, and 17 studies with insufficient data to construct two by two tables.

A total of 24 articles were collected [6, 10–32], each of which reported one or more modalities to classify prostate lesions into benign or malignant on the basis of imaging results. Two articles [24, 27] excluded from analysis lesions that were not seen by raters on T2-weighted imaging and were further excluded from this meta-analysis.

Twenty-two articles in total were included in the meta-analysis (Table 1), and each reported one or more imaging sequences, including DCE-MRI, to classify prostate lesions into benign or malignant on the basis of imaging results. Data from the 22 selected articles were extracted for information on study design, year of publication, number of patients, number of regions evaluated (total numbers and numbers positive for prostate cancer), scanner field strength, type of coil (external pelvic phased-array and endorectal coil), reference standard (whole-mount or step-section histopathology and transrectal ultrasound [TRUS] biopsy), method of DCE-MRI analysis (time-intensity curve, pharmacokinetic perfusion parameters, and color maps), anatomic zone of prostate evaluated (PZ, transition zone [TZ], and both), and number of raters.

For all studies included in the meta-analysis, the total number of lesions along with the number of true-positive, false-positive, true-negative, and false-negative lesions were

available for each study. When the number of lesions was not explicitly stated in an article, the sensitivity, specificity, and accuracy data were recorded and retrospectively analyzed on the basis of the reported number of sites. Where available, the results were recorded separately for sites (PZ, TZ, or PZ and TZ) and number of raters.

All data for which the two by two tables could be constructed were used for analysis. We did not exclude any part of the studies included in the meta-analysis. Thereby, a total of 25 raters and 1483 patients with 3520 lesions for DCE-MRI were included in the meta-analysis. The recorded variables for all included studies are presented in Table 1.

Statistical Analysis

Meta-analysis was implemented using data from all regions (TZ, PZ, PZ and TZ, and extra-capsular extension [ECE]), all regions excluding ECE, and separately for PZ and TZ. For the total dataset, if more than one location was reported in an article, only the data from PZ and TZ were used for analysis (which combined TZ and PZ).

A modality was included in the meta-analysis if reported in at least five articles for each specific dataset. For example, in the total dataset, 10 modalities were reported, five of them were not included in the analysis because of insufficient numbers of articles (one color Doppler ultrasound; two combined DWI and DCE-MRI; two MRS; three combined T2-weighted imaging and DWI, and one TRUS in total dataset). A total of five modalities were successfully analyzed: 16 DCE-MRI; 14 T2-weighted imaging; five combined DCE-MRI and T2-weighted imaging; seven DWI; and seven combined DCE-MRI, DWI, and T2-weighted imaging. Studies that relied on visual analysis to diagnose disease on DCE-MRI were analyzed separately from studies that relied on parametric DCE-MRI data (nonvisual analysis). A summary of the reviewed articles is provided in Table 2.

A binormal bayesian ROC model was used to estimate and compare sensitivity, specificity, AUC among eligible modalities [33, 34]. The model assumes that classification arises from unobserved gaussian random variables. The distribution of latent traits underlying conspicuity for malignant lesions is assumed to be $N(a, b)$, whereas traits for benign lesions are assumed to generate from a standard normal distribution, $N(0, 1)$. Posterior predictive checks were used to specify the final hyperparameters used in the analysis. Location parameters assumed zero-centered gaussian priors with precision of 0.01. Gamma priors were used for inverse variance hyperparameters with shape of 7 and rate of 1. Bayesian computation used Markov chain Monte Carlo simulation implemented using Open-BUGS software (version 3.2.1, R Project).

Comparisons between modalities were based on posterior 95% credible intervals. A significant difference was conferred between two modalities in the absence of overlap between credible intervals. Diagnostic accuracy was also compared through partial AUC restricted to the domain yielding at least 80% specificity because gains in sensitivity over this region have the most impact for actual clinical application.

Results

Table 3 summarizes the posterior distributions of AUC, partial AUC, and sensitivity and specificity by dataset and modality. In the total dataset (Figs. 1 and 2 and Table 3), on the basis of 95% posterior credible intervals for parameters, DCE-MRI (0.80–0.84), DWI (0.76–0.85), and combined DCE-MRI and T2-weighted imaging (0.79–0.87) overlapped, suggesting no difference, but yielded significantly better AUC than T2-weighted imaging alone (0.66–0.74). DCE-MRI and combined DCE-MRI and T2-weighted imaging yielded significantly better AUC than combined DCE-MRI, DWI, and T2-weighted imaging (0.67–0.77). The AUC of combined DCE-MRI, DWI, and T2-weighted imaging and T2-weighted imaging alone overlapped, suggesting no difference. T2-weighted imaging alone (0.40–0.51) yielded significantly lower sensitivity than combined DCE-MRI, DWI, and T2-weighted imaging (0.52–0.62). The specificity for all modalities overlapped.

Combined DCE-MRI, DWI, and T2-weighted imaging yielded significantly better partial AUC, defined as 80% or greater specificity, (0.110, 0.103–0.117) than DCE-MRI (0.075, 0.069–0.081), T2-weighted imaging (0.078, 0.073–0.083), or DWI alone (0.088, 0.079–0.095). However, no significant difference was seen compared with combined DCE-MRI and T2-weighted imaging (0.091, 0.077–0.104) (Figs. 1 and 2 and Table 3).

When ECE was removed from the dataset (Table 3) to enable evaluation of lesion detection within the prostate, similar findings were noted as with the total dataset; however, combined DCE-MRI and T2-weighted imaging could not be evaluated because of insufficient data.

In subset analysis of data reporting PZ and TZ separately (Figs. 3 and 4 and Table 3), combined DCE-MRI and T2-weighted imaging could not be evaluated because of insufficient data. In this subset, generally similar findings were noted as with the total dataset. However, DCE-MRI (0.82–0.86); DWI (0.84–0.88); and combined DCE-MRI, DWI, and T2-weighted imaging (0.73–0.88) yielded similar AUC instead of the first two showing superiority to the triple combination. No difference in sensitivity was noted among the modalities, including no difference between T2-weighted imaging and combined DCE-MRI, DWI, and T2-weighted imaging. The partial AUC of combined DCE-MRI, DWI, and T2-weighted imaging (0.103–0.109) was again noted be superior to T2-weighted imaging (0.074–0.084) and DCE-MRI (0.072–0.085), but similar to DWI (0.091–0.108).

PZ and TZ could not be analyzed and compared separately because of too few articles in each subgroup. For the PZ-only dataset (Table 3), only results from DCE-MRI alone were deemed suitable for analysis.

Subgroup analysis of the total dataset found no difference between studies that used visual analysis of DCE-MRI findings versus nonvisual analysis, such as time-intensity curves or tracer kinetic models (Tables 1 and 3 and Fig. 5). Similar comparison could not be performed on the PZ and TZ dataset because the number of such studies for comparison was too small.

Discussion

DCE-MRI serves to show the perfusion parameters of tissues. It gathers information about the vascularity of tissues by assessing the signal intensity of tissues over time (dynamic) after IV administration of gadolinium contrast material. The micro-vascular alterations and neovascularity have been shown to be increased in prostate cancer in comparison with other processes, such as BPH or prostatic intraepithelial neoplasia [35]. Additionally, prognosis may worsen as the microvessel density in prostate cancer increases; the latter often correlates with DCE-MRI findings, such as reverse reflux rate constant between extracellular space and plasma (K_{ep}) [36–38]. In the current meta-analysis, we noted that the AUC of DCE-MRI alone or combined DCE-MRI and T2-weighted imaging was found to be superior to T2-weighted imaging alone, which was the prior standard method for detecting prostate cancer before multiparametric imaging.

DCE-MRI has several strengths for implementation in clinical practice. Using high-temporal-resolution gradient-recalled echo (GRE) T1-weighted imaging, consecutive runs of the same sequence may be performed in the prostate gland without the adverse effects of ionizing radiation that may be encountered on CT. Extracellular gadolinium chelate agents are the mainstay in DCE-MRI, and other than for recent concerns with nephrogenic systemic fibrosis (NSF) in advanced renal impairment, these chelates are safe to administer [39]. Importantly, DCE-MRI can be easily performed in patients on most clinical MRI scanners. Unlike in MRS in which scanning times are long [40], often on the order of 15–20 minutes, a routine DCE-MRI sequence typically requires only an additional 5 minutes of scanning.

The main limitation of DCE-MRI is that, at present, there is no consensus as to the optimal method of assessing perfusion because there is often a conflict between complexity and standardization [41]. The simplest method and most easily standardized approach will be the visual method, in which one looks for areas that show rapid enhancement and deenhancement or washout. This assumes that the signal intensity of the image is proportional to the concentration of gadolinium contrast agent in the tissues and that it is directly related to abnormal vasculature of the tumor.

To make the analysis more technical but less subject to intraobserver and interobserver variability, a semiquantitative method would be to use time-intensity curves. Using this method, the time of first contrast uptake, time to peak, maximum slope, peak enhancement, and wash-in and washout curve shapes can be derived. It has been suggested in several studies that malignant lesions consistently show high signal intensity amplitudes with early wash-in and rapid washout on time-intensity curves; it has been suggested that this method may even serve to improve diagnosis in less-experienced readers [13].

However, proponents of quantitative analysis would consider these methods oversimplification because they do not take into account other factors that influence signal intensity, including that MRI signal intensity is not linear with the gadolinium concentration and that gadolinium contrast agents freely diffuse across the vessel wall and into the extracellular matrix (extravascular-extracellular volume denoted by the parameter, V_e), according to the permeability of the vessels (permeability constant). Hence, to accurately

define the common perfusion parameters, such as K^{trans} (forward volume transfer constant) and K_{ep} (reverse reflux rate constant between extracellular space and plasma), a significant amount of postprocessing is required. Various mathematic models have been developed to quantify perfusion; the Tofts model of pharmacokinetic-tracer dynamic analysis [42] is perhaps the most widely applied.

To further complicate matters, there are at present no standard objective cutoff values among the perfusion parameters that have been described for determining whether a lesion is malignant, whereas a significant overlap between prostate cancer and benign entities, such as BPH nodules, exists [43]. To enable more efficient practice, color-coded maps using predefined cutoff values or time-intensity curves that are superimposed on anatomic T2-weighted images can be created to enable radiologists to evaluate the prostate gland for suspicious foci more quickly. Thus, semiquantitative analysis is still undergoing optimization. In our study, we did not find a significant difference between visual and nonvisual DCE-MRI analysis methods.

Comparing our current results to a prior meta-analysis [34] that we conducted on DWI for prostate cancer diagnosis, which included 19 articles and a total of 5892 lesions (which was fairly comparable to our current study on DCE-MRI in which we included 22 articles and a total of 3520 lesions), partial AUC for the PZ and TZ datasets is better for DWI (0.121–0.136, 0.091–0.108 for the previous article and the current article, respectively) than DCE-MRI (0.070–0.090, 0.072– 0.085, respectively).

Direct comparison with the results of the prior analysis for the diagnostic performance of T2-weighted imaging, DWI, or DCE-MRI should not be made because of the different inclusion and exclusion criteria. Nevertheless, qualitative comparison of the trends shows similar findings between the two studies of superiority of DWI or at least equivalency of DWI compared with DCE-MRI. In both studies, the AUC of DWI or DCE-MRI was superior to T2-weighted imaging and partial AUC of DWI was superior to partial AUC of T2-weighted imaging. Qualitative comparison showed that AUCs and partial AUCs for DCE-MRI were similar between the two meta-analyses.

In the total dataset of the current study, DCE-MRI (0.80–0.84) and combined DCE-MRI and T2-weighted imaging (0.79–0.87) AUCs were superior to combined DCE-MRI, DWI, and T2-weighted imaging (0.67–0.77), but by partial AUC, the triple combination was better than DCE-MRI (0.069–0.081 vs 0.103–0.117 for the triple combination) but not combined DCE-MRI and T2-weighted imaging (0.077–0.104). Our findings suggest that combined DCE-MRI and T2-weighted imaging performs similar to DCE-MRI overall and at specificities of 80% or greater. Our findings also suggest that combined DCE-MRI and T2-weighted imaging performs better than combined DCE-MRI, DWI, and T2-weighted imaging overall (AUC) and similarly at specificities of 80% or greater.

In the total dataset, the AUC of DWI (0.76–0.85) was similar to combined DCE-MRI and T2-weighted imaging (0.79–0.87) and combined DCE-MRI, DWI, and T2-weighted imaging (0.67–0.77) and the partial AUC of DWI (0.079–0.095) was similar to combined DCE-MRI and T2-weighted imaging (0.077–0.104) but less than combined DCE-MRI,

DWI, and T2-weighted imaging (0.103–0.117). In the PZ and TZ dataset, the AUC and partial AUC of DWI (0.84–0.88 and 0.091–0.108, respectively) was similar to combined DCE-MRI, DWI, and T2-weighted imaging (0.73–0.88 and 0.103– 0.109, respectively). Thus, DWI appears to perform similar to combined DCE-MRI and T2-weighted imaging and DCE-MRI, DWI, and T2-weighted imaging. In our prior study [34], DWI was superior to combined DWI and T2-weighted imaging by AUC (0.82–0.87 vs 0.71–0.75) but similar by partial AUC (0.121–0.136 vs 0.134–0.140). Thus, the predominant factor appears to be DWI, and it is likely responsible for any gains seen by combination imaging of T2-weighted imaging with DWI or T2-weighted imaging, DWI, and DCE-MRI versus T2-weighted imaging or DCE-MRI alone. Moreover, there does not appear to be a clear advantage of double multiparametric imaging (DWI and T2-weighted imaging or DCE-MRI and T2-weighted imaging) versus triple (DCE-MRI, DWI, and T2-weighted imaging). The findings are supported by Vilanova et al. [44] who suggested that combined DWI and T2-weighted imaging and not combined T2-weighted imaging, DWI, and DCE-MRI may be a modality of choice given the additional scanning times, contrast administration, and lack of significant improvement in diagnostic accuracy in combined T2-weighted imaging, DWI, and DCE-MRI. T2-weighted imaging remains an essential component of prostate cancer imaging for anatomic information and for visualizing involvement of adjacent structures, such as the seminal vesicles and neurovascular bundles.

Future research will concentrate not just on improving tumor detection but also on local staging, treatment response assessment, and ability of MRI to guide biopsy and subsequent management of patients. That has not been addressed in our current meta-analysis. On the basis of early studies, DCE-MRI has shown promising results for detection of recurrent disease after external beam radiotherapy [45] as well as after radical prostatectomy [46].

The most important limitation of this study lies in the heterogeneity in the methods of analysis of perfusion imaging data for diagnosis of prostate cancer. As with DWI, there is currently no consensus on the best method of analyzing DCE-MRI data after it is obtained. As alluded to earlier, DCE-MRI data can be interpreted visually, semiquantitatively (using time-intensity curves), or quantitatively. Among the 22 studies that were included in our meta-analysis, seven used visual assessment and the rest used nonvisual methods, such as time-intensity curves or color maps derived from K^{trans}, $K_{ep,}$ or V_e (Table 1). To reduce the effects of such heterogeneity, we have deliberately used each individual article's semiquantitative data cutoff as positive or negative for cancer so that variance in cutoff does not affect sensitivity and specificity in terms of statistical analysis for the meta-analysis. We further performed a subgroup analysis of the studies that relied on the qualitative method of interpreting DCE-MRI data and those that relied on the quantitative method interpreting DCE-MRI data. In doing so, we found that the results for the two subgroups were essentially similar.

Another limitation of this study lies in the varying temporal resolutions of the DCE-MRI sequences. All studies used GRE T1-weighted imaging for DCE-MRI. The spatial resolutions were also fairly similar. However, the temporal resolutions that are quoted in the articles ranged from 2 to 95 seconds. On the basis of the European consensus guideline recommendations for performance of DCE-MRI, the optimal temporal resolution for a

single run should be no more than 15 seconds [47]. This enables accurate determination of early wash in of gadolinium contrast material. Nevertheless, temporal resolutions greater than 15 seconds may be acceptable, provided tissue T1 relaxation times and arterial input functions are properly estimated [41].

Other than for the performance of the DCE-MRI sequences, technical factors that may influence the results of perfusion imaging, such as rate of contrast media injection and patients' hemodynamic status, were also not considered among the exclusion criteria for our study. Importantly, it may not be possible to ensure that all parameters are kept constant.

It is not possible to ensure uniformity in terms of the patient selection because both retrospective and prospective studies were included in this meta-analysis. To improve this limitation, we excluded studies that evaluated DCE-MRI in terms of its ability to assess treatment response and guide targeted biopsies of the prostate. We also excluded studies that retrospectively applied prefabricated ROI maps based on histopathology or T2-weighted imaging datasets to test the true diagnostic value of DCE-MRI. The local staging accuracy of DCE-MRI for disease in the TZ only, ECE, and seminal vesicles invasion was also not addressed in this meta-analysis because of the lack of data. It has been suggested from the limited evidence that combined DCE-MRI and T2-weighted imaging may play a role in local staging assessment by improving detection of ECE [15].

Lastly, we were not able to perform analyses comparing DCE-MRI to modalities other than T2-weighted imaging and DWI alone because of insufficient studies with those modalities. The reason may be that the search terms were focused on “dynamic contrast-enhanced MRI” rather than on other techniques using multiparametric MRI, such as combined DWI and T2-weighted imaging or MRS. Prior studies [44, 48] have not found statistical evidence of improved diagnostic parameters with use of three instead of two multiparametric parameters. The marginal improvement with DCE-MRI suggests that two parameters, such as T2-weighted imaging combined with DWI, may be sufficient for clinical practice. In certain situations, such as locating lesions for biopsy, adding DCE-MRI may give confidence in picking a target lesion, but further statistical studies of benefit in this regard are needed.

Conclusion

Dynamic contrast-enhanced MRI improves AUC of tumor detection overall compared with T2-weighted imaging alone. Methods for DCE-MRI analysis require standardization, but visual analysis performs similar to semiquantitative methods. A two-parameter approach using combined DCE-MRI and T2-weighted imaging or combined DWI and T2-weighted imaging may be sufficient, and the latter may be more favorable for most routine prostate cancer imaging.

References

1. Mazaheri Y, Shukla-Dave A, Muellner A, Hricak H. MR imaging of the prostate in clinical practice. MAGMA. 2008; 21:379–392. [PubMed: 18795354]
2. Sonnad SS, Langlotz CP, Schwartz JS. Accuracy of MR imaging for staging prostate cancer: a meta-analysis to examine the effect of technologic change. Acad Radiol. 2001; 8:149–157. [PubMed: 11227643]

3. Engelbrecht MR, Huisman HJ, Laheij RJ, et al. Discrimination of prostate cancer from normal peripheral zone and central gland tissue by using dynamic contrast-enhanced MR imaging. Radiology. 2003; 229:248–254. [PubMed: 12944607]

4. Bonekamp D, Jacobs MA, El-Khouli R, Stoianovici D, Macura KJ. Advancements in MR imaging of the prostate: from diagnosis to interventions. RadioGraphics. 2011; 31:677–703. [PubMed: 21571651]

5. Tanimoto A, Nakashima J, Kohno H, Shinmoto H, Kuribayashi S. Prostate cancer screening: the clinical value of diffusion-weighted imaging and dynamic MR imaging in combination with T2-weighted imaging. J Magn Reson Imaging. 2007; 25:146–152. [PubMed: 17139633]

6. Turkbey B, Pinto PA, Mani H, et al. Prostate cancer: value of multiparametric MR imaging at 3 T for detection—histopathologic correlation. Radiology. 2010; 255:89–99. [PubMed: 20308447]

7. Fenner A. Prostate cancer: multiparametric MRI scans could be a useful adjunct for active surveillance in prostate cancer. Nat Rev Urol. 2013; 10:247. [PubMed: 23528701]

8. Liberati A, Altman DG, Tetzlaff J, et al. The PRISMA statement for reporting systematic reviews and meta-analyses of studies that evaluate health care interventions: explanation and elaboration. J Clin Epidemiol. 2009; 62:e1–e34. [PubMed: 19631507]

9. Moher D, Liberati A, Tetzlaff J, Altman DG. Preferred reporting items for systematic reviews and meta-analyses: the PRISMA statement. J Clin Epidemiol. 2009; 62:1006–1012. [PubMed: 19631508]

10. Jager GJ, Ruijter ET, van de Kaa CA, et al. Dynamic turboFLASH subtraction technique for contrast-enhanced MR imaging of the prostate: correlation with histopathologic results. Radiology. 1997; 203:645–652. [PubMed: 9169683]

11. Ogura K, Maekawa S, Okubo K, et al. Dynamic endorectal magnetic resonance imaging for local staging and detection of neurovascular bundle involvement of prostate cancer: correlation with histopathologic results. Urology. 2001; 57:721–726. [PubMed: 11306390]

12. Ito H, Kamoi K, Yokoyama K, Yamada K, Nishimura T. Visualization of prostate cancer using dynamic contrast-enhanced MRI: comparison with transrectal power Doppler ultrasound. Br J Radiol. 2003; 76:617–624. [PubMed: 14500276]

13. Fütterer JJ, Engelbrecht MR, Huisman HJ, et al. Staging prostate cancer with dynamic contrast-enhanced endorectal MR imaging prior to radical prostatectomy: experienced versus less experienced readers. Radiology. 2005; 237:541–549. [PubMed: 16244263]

14. Kim CK, Park BK, Kim B. Localization of prostate cancer using 3T MRI: comparison of T2-weighted and dynamic contrast-enhanced imaging. J Comput Assist Tomogr. 2006; 30:7–11. [PubMed: 16365565]

15. Bloch BN, Furman-Haran E, Helbich TH, et al. Prostate cancer: accurate determination of extracapsular extension with high-spatial-resolution dynamic contrast-enhanced and T2-weighted MR imaging—initial results. Radiology. 2007; 245:176–185. [PubMed: 17717328]

16. Yu JS, Chung JJ, Hong SW, Chung BH, Kim JH, Kim KW. Prostate cancer: added value of subtraction dynamic imaging in 3T magnetic resonance imaging with a phased-array body coil. Yonsei Med J. 2008; 49:765–774. [PubMed: 18972597]

17. Puech P, Huglo D, Petyt G, Lemaitre L, Villers A. Imaging of organ-confined prostate cancer: functional ultrasound, MRI and PET/computed tomography. Curr Opin Urol. 2009; 19:168–176. [PubMed: 19188771]

18. Kitajima K, Kaji Y, Fukabori Y, Yoshida K, Suganuma N, Sugimura K. Prostate cancer detection with 3 T MRI: comparison of diffusion-weighted imaging and dynamic contrast-enhanced MRI in combination with T2-weighted imaging. J Magn Reson Imaging. 2010; 31:625–631. [PubMed: 20187206]

19. Tamada T, Sone T, Higashi H, et al. Prostate cancer detection in patients with total serum prostate-specific antigen levels of 4–10 ng/mL: diagnostic efficacy of diffusion-weighted imaging, dynamic contrast-enhanced MRI, and T2-weighted imaging. AJR. 2011; 197:664–670. [PubMed: 21862809]

20. Iwazawa J, Mitani T, Sassa S, Ohue S. Prostate cancer detection with MRI: is dynamic contrast-enhanced imaging necessary in addition to diffusion-weighted imaging? Diagn Interv Radiol. 2011; 17:243–248. [PubMed: 20859852]

21. Chabanova E, Balslev I, Logager V, et al. Prostate cancer: 1.5 T endo-coil dynamic contrast-enhanced MRI and MR spectroscopy—correlation with prostate biopsy and prostatectomy histopathological data. Eur J Radiol. 2011; 80:292–296. [PubMed: 20708869]
22. Novis MI, Baroni RH, Cerri LM, Mattedi RL, Buchpiguel CA. Clinically low-risk prostate cancer: evaluation with transrectal Doppler ultrasound and functional magnetic resonance imaging. Clinics (Sao Paulo). 2011; 66:27–34. [PubMed: 21437432]
23. Bloch BN, Genega EM, Costa DN, et al. Prediction of prostate cancer extracapsular extension with high spatial resolution dynamic contrast-enhanced 3-T MRI. Eur Radiol. 2012; 22:2201–2210. [PubMed: 22661019]
24. Fütterer JJ, Heijmink SW, Scheenen TW, et al. Prostate cancer localization with dynamic contrast-enhanced MR imaging and proton MR spectroscopic imaging. Radiology. 2006; 241:449–458. [PubMed: 16966484]
25. Tamada T, Sone T, Jo Y, et al. Prostate cancer: relationships between postbiopsy hemorrhage and tumor detectability at MR diagnosis. Radiology. 2008; 248:531–539. [PubMed: 18539890]
26. Rosenkrantz AB, Mussi TC, Hindman N, et al. Impact of delay after biopsy and post-biopsy haemorrhage on prostate cancer tumour detection using multi-parametric MRI: a multi-reader study. Clin Radiol. 2012; 67:e83–e90. [PubMed: 22981729]
27. Aydin H, Kizilgoz V, Tatar IG, et al. Detection of prostate cancer with magnetic resonance imaging: optimization of T1-weighted, T2-weighted, dynamic-enhanced T1-weighted, diffusion-weighted imaging apparent diffusion coefficient mapping sequences and MR spectroscopy, correlated with biopsy and histopathological findings. J Comput Assist Tomogr. 2012; 36:30–45. [PubMed: 22261768]
28. Soylu FN, Eggener S, Oto A. Local staging of prostate cancer with MRI. Diagn Interv Radiol. 2012; 18:365–373. [PubMed: 22399364]
29. Kozlowski P, Chang SD, Jones EC, Berean KW, Chen H, Goldenberg SL. Combined diffusion-weighted and dynamic contrast-enhanced MRI for prostate cancer diagnosis: correlation with biopsy and histopathology. J Magn Reson Imaging. 2006; 24:108–113. [PubMed: 16767709]
30. Min BD, Kim WT, Cho BS, et al. Usefulness of a combined approach of T1-weighted, T2-weighted, dynamic contrast-enhanced, and diffusion-weighted imaging in prostate cancer. Korean J Urol. 2012; 53:830–835. [PubMed: 23301126]
31. Hoeks CM, Hambrock T, Yakar D, et al. Transition zone prostate cancer: detection and localization with 3-T multiparametric MR imaging. Radiology. 2013; 266:207–217. [PubMed: 23143029]
32. Van den Bergh L, Isebaert S, Koole M, et al. Does ^{11}C-choline PET-CT contribute to multiparametric MRI for prostate cancer localisation? Strahlenther Onkol. 2013; 189:789–795. [PubMed: 23797481]
33. Johnson, VE.; Albert, JH. Ordinal data modeling. New York, NY: Springer-Verlag; 1999.
34. Tan CH, Wei W, Johnson V, Kundra V. Diffusion-weighted MRI in the detection of prostate cancer: meta-analysis. AJR. 2012; 199:822–829. [PubMed: 22997374]
35. Padhani AR, Harvey CJ, Cosgrove DO. Angiogenesis imaging in the management of prostate cancer. Nat Clin Pract Urol. 2005; 2:596–607. [PubMed: 16474547]
36. Erbersdobler A, Isbarn H, Dix K, et al. Prognostic value of microvessel density in prostate cancer: a tissue microarray study. World J Urol. 2010; 28:687–692. [PubMed: 19714336]
37. Brawer MK. Prostate cancer detection. J Urol. 1994; 151:1308–1309. [PubMed: 8158776]
38. Oto A, Yang C, Kayhan A, et al. Diffusion-weighted and dynamic contrast-enhanced MRI of prostate cancer: correlation of quantitative MR parameters with Gleason score and tumor angiogenesis. AJR. 2011; 197:1382–1390. [PubMed: 22109293]
39. Deray G, Rouviere O, Bacigalupo L, et al. Safety of meglumine gadoterate (Gd-DOTA)-enhanced MRI compared to unenhanced MRI in patients with chronic kidney disease (RESCUE study). Eur Radiol. 2013; 23:1250–1259. [PubMed: 23212275]
40. Choi YJ, Kim JK, Kim N, Kim KW, Choi EK, Cho KS. Functional MR imaging of prostate cancer. RadioGraphics. 2007; 27:63–75. discussion, 75–77. [PubMed: 17234999]
41. Verma S, Turkbey B, Muradyan N, et al. Overview of dynamic contrast-enhanced MRI in prostate cancer diagnosis and management. AJR. 2012; 198:1277–1288. [PubMed: 22623539]

42. Tofts PS, Wicks DA, Barker GJ. The MRI measurement of NMR and physiological parameters in tissue to study disease process. Prog Clin Biol Res. 1991; 363:313–325. [PubMed: 1988983]
43. Oto A, Kayhan A, Jiang Y, et al. Prostate cancer: differentiation of central gland cancer from benign prostatic hyperplasia by using diffusion-weighted and dynamic contrast-enhanced MR imaging. Radiology. 2010; 257:715–723. [PubMed: 20843992]
44. Vilanova JC, Barcelo-Vidal C, Comet J, et al. Usefulness of prebiopsy multifunctional and morphologic MRI combined with free-to-total prostate-specific antigen ratio in the detection of prostate cancer. AJR. 2011; 196:W715–W722. web. [PubMed: 21606259]
45. Haider MA, Chung P, Sweet J, et al. Dynamic contrast-enhanced magnetic resonance imaging for localization of recurrent prostate cancer after external beam radiotherapy. Int J Radiat Oncol Biol Phys. 2008; 70:425–430. [PubMed: 17881141]
46. Casciani E, Polettini E, Carmenini E, et al. Endorectal and dynamic contrast-enhanced MRI for detection of local recurrence after radical prostatectomy. AJR. 2008; 190:1187–1192. [PubMed: 18430830]
47. Dickinson L, Ahmed HU, Allen C, et al. Magnetic resonance imaging for the detection, localisation, and characterisation of prostate cancer: recommendations from a European consensus meeting. Eur Urol. 2011; 59:477–494. [PubMed: 21195536]
48. Riches SF, Payne GS, Morgan VA, et al. MRI in the detection of prostate cancer: combined apparent diffusion coefficient, metabolite ratio, and vascular parameters. AJR. 2009; 193:1583–1591. [PubMed: 19933651]

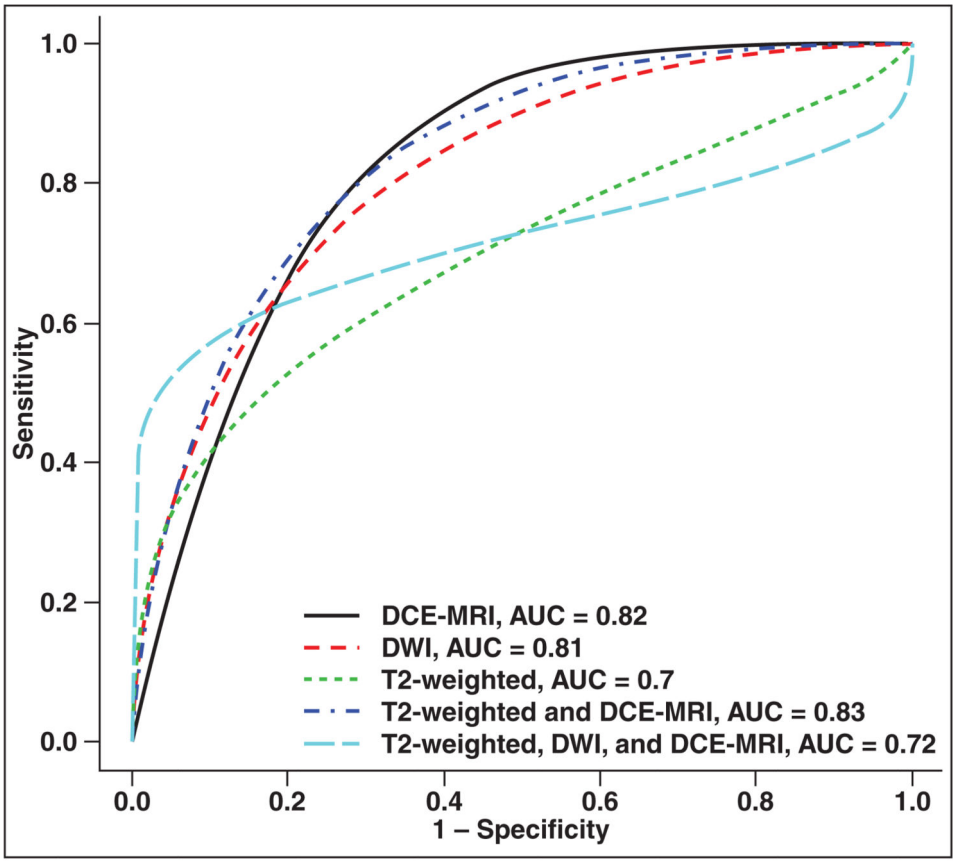

Fig. 1.

ROC curves show each modality derived from combined data. DCE-MRI = dynamic contrast-enhanced MRI, DWI = diffusion-weighted MRI.

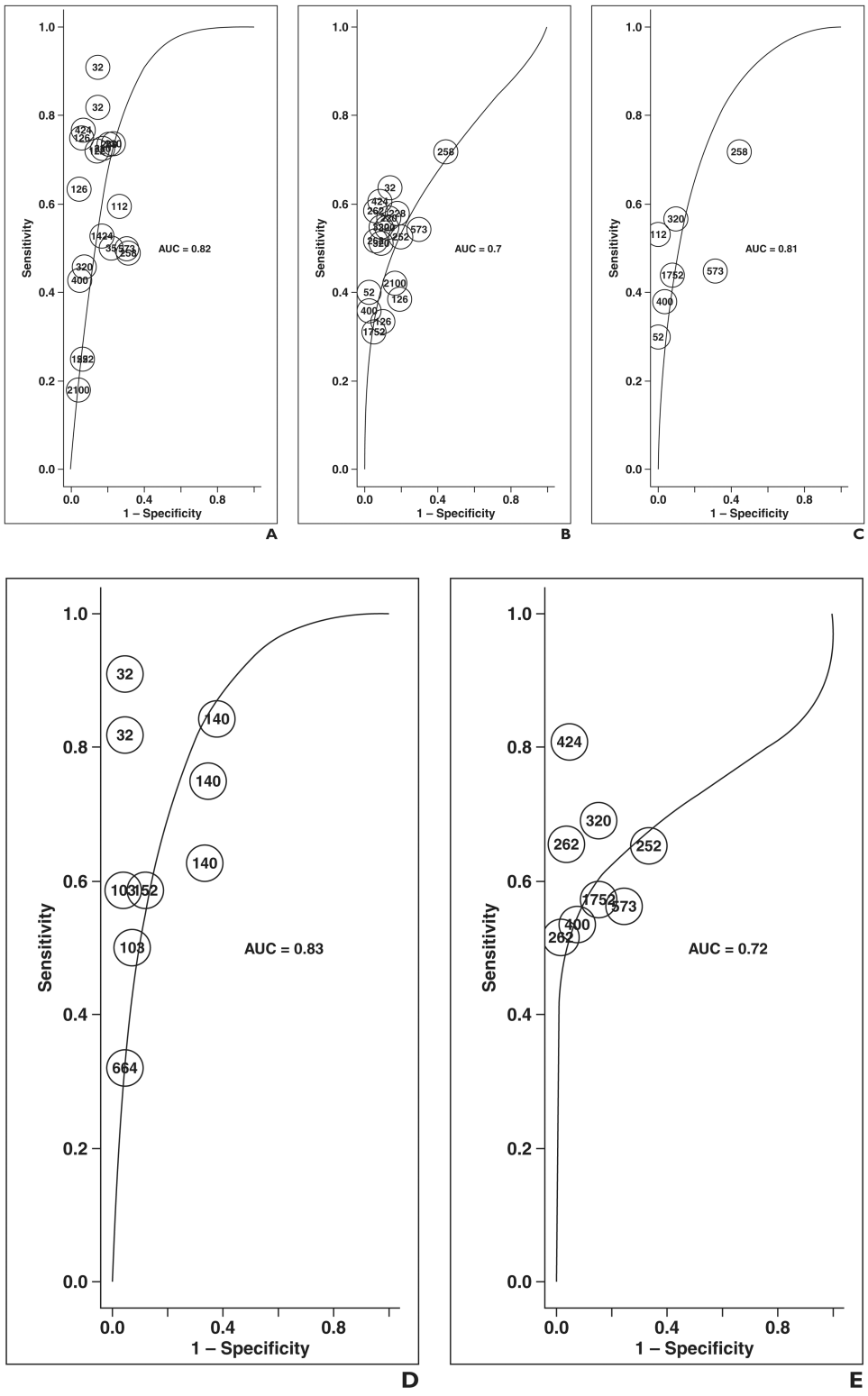

Fig. 2.
ROC curves show combined data.

A–E, On graphs for dynamic contrast-enhanced (DCE-MRI) imaging (**A**); T2-weighted imaging (**B**); diffusion-weighted MRI (DWI) (**C**); combined T2-weighted and DCE-MRI (**D**); and combined T2-weighted, DWI, and DCE-MRI (**E**); each point represents contribution of single rater on basis of number of lesions evaluated.

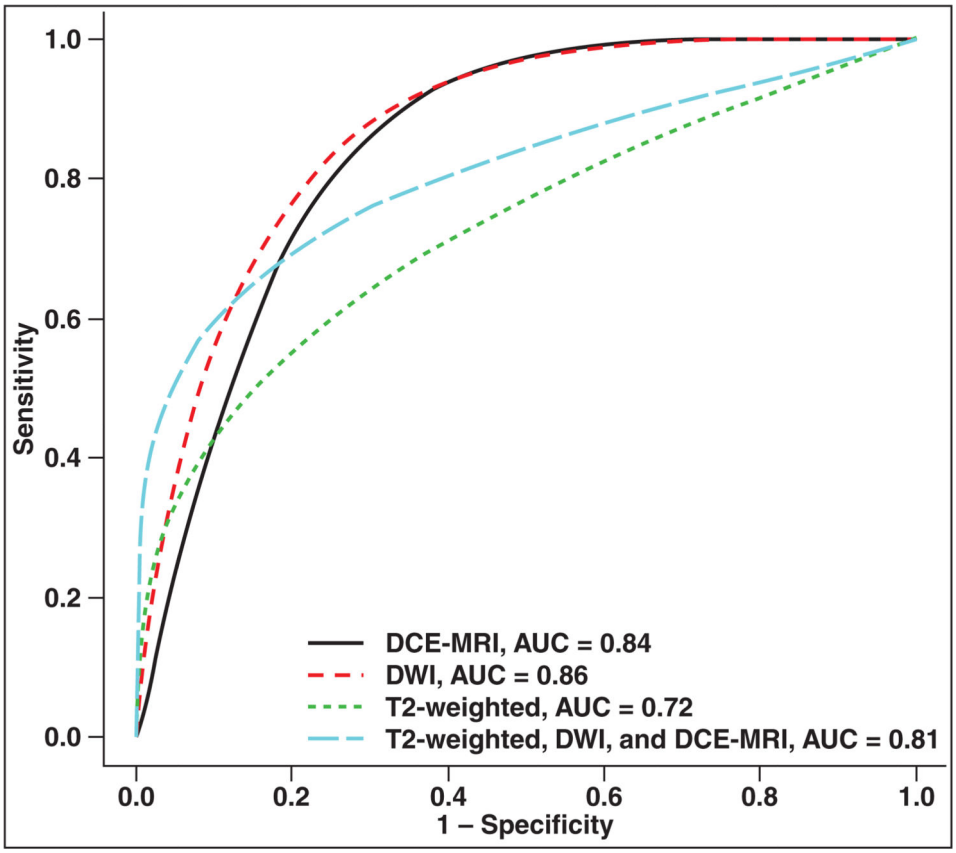

Fig. 3.

ROC curves show each modality for peripheral zone and transition zone only. DCE-MRI = dynamic contrast-enhanced MRI, DWI = diffusion-weighted MRI.

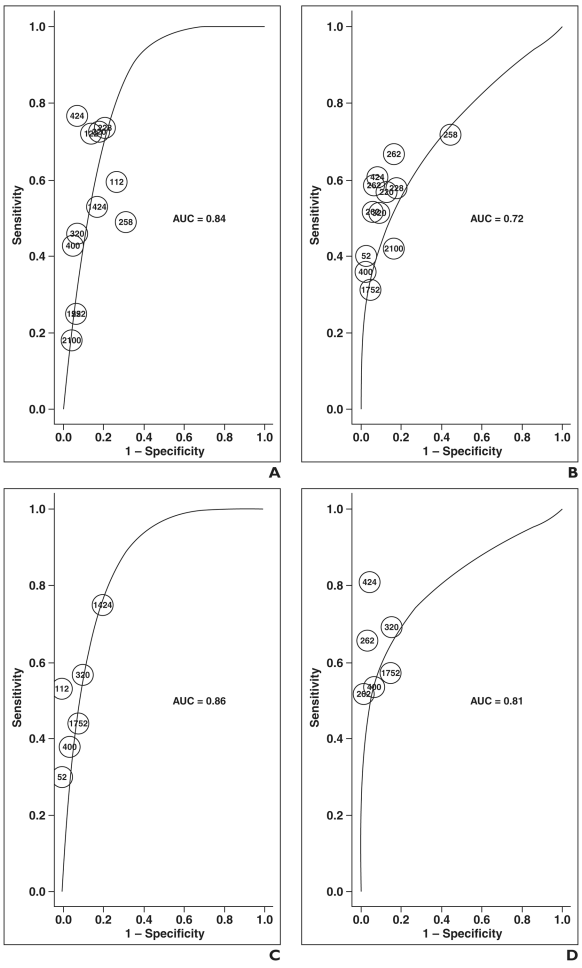

Fig. 4.

ROC curves show peripheral zone and transition zone data.

A–D, On graphs for dynamic contrast-enhanced (DCE-MRI) imaging (**A**); T2-weighted imaging (**B**); diffusion-weighted MRI (DWI) (**C**); and combined T2-weighted, DWI, and DCE-MRI (**D**); each point represents contribution of single rater on basis of number of lesions evaluated.

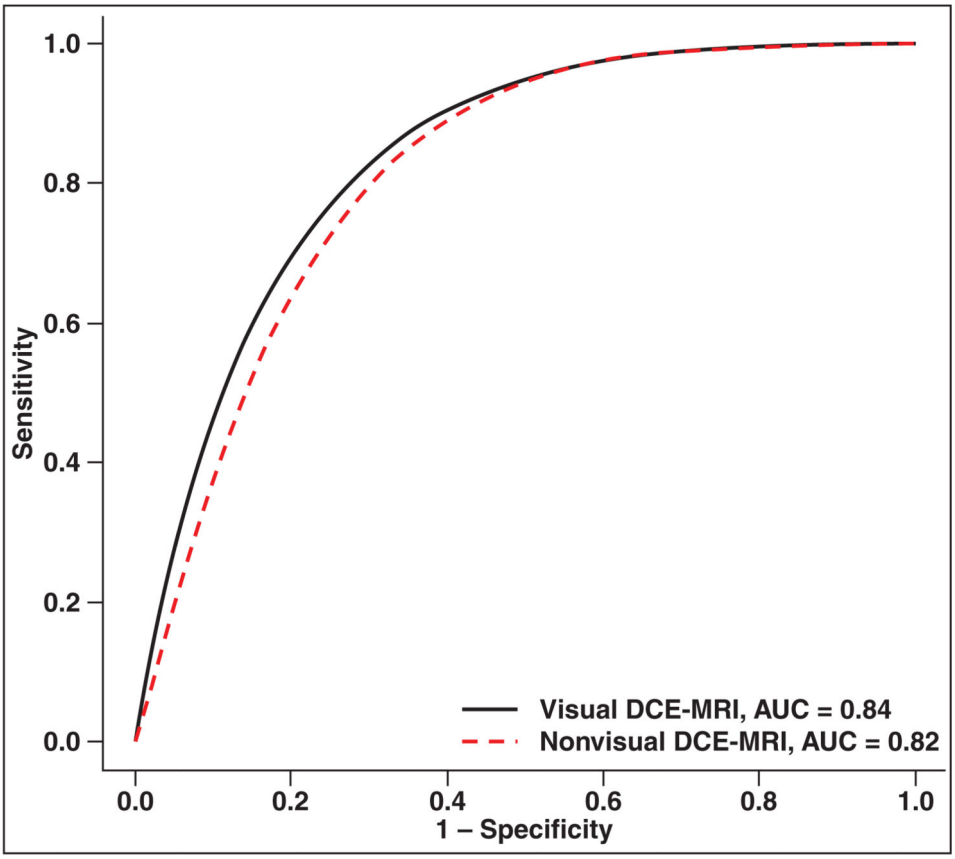

Fig. 5.

ROC curves show visual versus semiquantitative assessment of dynamic contrast-enhanced MRI (DCE-MRI).

Table 1

List of Articles Selected for Meta-Analysis and Data Recorded

No.	First Author [Reference No.]	Year	No. of Patients	No. of Regions	No. of Positive Regions	Scanner Field Strength (T)	Type of Coil	Slice Thickness (mm)	Reference Standard	Method of Analysis	Anatomic Zone Evaluated	No. of Raters
1	Turkbey [6]	2010	70	2100	628	3	Endorectal	6	Whole-mount histopathology	Nonvisual	PZ and TZ	2 (consensus)
2	Jager [10]	1997	57	228	102	1.5	Endorectal	10	Step-section histopathology	Nonvisual	PZ, TZ, PZ and TZ	2
3	Ogura [11]	2001	38	152	85	1.5	Endorectal	6	Whole-mount histopathology	Visual	PZ, TZ, PZ and TZ	2 (consensus)
4	Ito [12]	2003	31	122	64	1.5	Torso phased-array	4	TRUS	Nonvisual	PZ, TZ, PZ and TZ	2 (consensus)
5	Fütterer [13]	2005	99	99	34	1.5	Endorectal	7	Whole-mount histopathology	Nonvisual	ECE	2
6	Kim [14]	2006	20	120	64	3	Torso phased-array	3	TRUS	Visual	PZ only	2 (consensus)
7	Bloch [15]	2012	108	108	32	3	Endorectal	3	Whole-mount histopathology	Nonvisual	ECE	2
8	Yu [16]	2008	21	126	60	3	Torso phased-array	4	Whole-mount histopathology	Visual	PZ only	2
9	Puech [17]	2009	83	664	212	1.5	Torso phased-array	4	Whole-mount histopathology	Visual	PZ and TZ	2 (consensus)
10	Kitajima [18]	2010	53	424	99	3	Torso phased-array	3	TRUS	Nonvisual	PZ and TZ	2 (consensus)
11	Tamada [19]	2011	50	400	103	1.5	phased-array Torso	5	TRUS	Visual	PZ and TZ	2 (consensus)
12	Iwazawa [20]	2011	178	1424	318	1.5	Torso phased-array	2.5	TRUS	Visual	PZ, TZ, PZ and TZ	2 (consensus)
13	Chabanova [21]	2011	43	258	149	1.5	Endorectal	6.5	Step-section histopathology	Nonvisual	PZ and TZ	1
14	Novis [22]	2011	35	35	8	1.5	Endorectal	3	Step-section histopathology	Nonvisual	ECE	2
15	Fütterer [24]	2006	34	479	112	1.5	Endorectal	4	Whole-mount histopathology	Nonvisual	PZ and TZ	2
16	Tamada [25]	2008	40	320	129	1.5	Torso phased-array	5	TRUS	Visual	PZ and TZ	3 (consensus)
17	Rosenkrantz [26]	2012	44	573	303	1.5	Torso phased-array	2	Step-section histopathology	Nonvisual	PZ only	3 (consensus)
18	Soylu [28]	2013	131	262	29	1.5	Endorectal	3	Whole-mount histopathology	Nonvisual	PZ and TZ	2
19	Kozlowski [29]	2006	14	112	32	1.5	Endorectal	5	Whole-mount histopathology	Nonvisual	PZ and TZ	2
20	Min [30]	2012	126	NA	NA	3	Torso phased-array	2	Whole-mount histopathology	Nonvisual	PZ and TZ	1
21	Hoeks [31]	2013	63	252	112	37	Endorectal	3	Whole-mount histopathology	Nonvisual	TZ	4
22	Van den Bergh [32]	2013	73	1752	708	1.5	Torso phased-array	4	Whole-mount histopathology	Nonvisual	PZ and TZ	1

Note—PZ = peripheral zone, TZ = transition zone, TRUS = transrectal ultrasound, ECE = extracapsular extension, NA = not applicable.

Table 2

Summary of Articles Reviewed

Modality	No. of Articles	No. of Raters	No. of Regions
Color Doppler ultrasound	1	1	122
DCE-MRI	16	19	8384
DWI	7	7	4553
DCE-MRI and DWI	2	2	1456
MRS	2	2	2358
T2-weighted imaging	14	18	7547
DCE-MRI and T2-weighted imaging	5	9	1402
DWI and T2-weighted imaging	3	4	1200
DCE-MRI, DWI, and T2-weighted imaging	7	8	4245
TRUS	1	1	35

Note—DCE-MRI = dynamic contrast-enhanced MRI, DWI = diffusion-weighted MRI, MRS = MR spectroscopy, TRUS = transrectal ultrasound.

Table 3

Posterior Means and 95% Credible Intervals for AUC, Partial AUC, Sensitivity, and Specificity

Dataset	Modality	No. of Articles (Raters)	Posterior Mean (95% Credible Interval)			
			AUC	Partial AUC (80% Specificity or Higher)	Sensitivity	Specificity
Total with ECE	DCE-MRI	16 (19)	0.82 (0.80–0.84)	0.075 (0.069–0.081)	0.55 (0.45–0.65)	0.85 (0.81–0.89)
	T2-weighted imaging	14 (18)	0.70 (0.66–0.74)	0.078 (0.073–0.083)	0.46 (0.40–0.51)	0.87 (0.82–0.91)
	DCE-MRI, T2-weighted imaging	5 (9)	0.83 (0.79–0.87)	0.091 (0.077–0.104)	0.64 (0.50–0.77)	0.83 (0.75–0.90)
	DWI	7 (7)	0.81 (0.76–0.85)	0.088 (0.079–0.095)	0.46 (0.33–0.6)	0.90 (0.84–0.95)
	DCE-MRI, DWI, and T2-weighted imaging	7 (8)	0.72 (0.67–0.77)	0.110 (0.103– 0.117)	0.57 (0.52–0.62)	0.89 (0.83–0.94)
Total without ECE	DCE-MRI	14 (16)	0.82 (0.80–0.84)	0.075 (0.069–0.081)	0.52 (0.42–0.63)	0.86 (0.81–0.90)
	T2-weighted imaging	13 (16)	0.82 (0.80–0.84)	0.075 (0.069–0.081)	0.52 (0.42–0.63)	0.86 (0.81–0.90)
	DCE-MRI, T2-weighted imaging	7 (7)	0.81 (0.76–0.85)	0.088 (0.079–0.095)	0.46 (0.33–0.60)	0.90 (0.84–0.95)
	DWI	7 (8)	0.72 (0.67–0.77)	0.110 (0.103– 0.117)	0.57 (0.52–0.62)	0.89 (0.83–0.94)
PZ and TZ	DCE-MRI	11 (12)	0.84 (0.82–0.86)	0.079 (0.072–0.085)	0.50 (0.36–0.64)	0.88 (0.83–0.92)
	T2-weighted imaging	9 (11)	0.72 (0.68–0.77)	0.079 (0.074–0.084)	0.45 (0.37–0.53)	0.88 (0.82–0.93)
	DCE-MRI, T2-weighted imaging	6 (6)	0.86 (0.84–0.88)	0.099 (0.091–0.108)	0.47 (0.30–0.65)	0.92 (0.86–0.96)
	DWI	5 (6)	0.81 (0.73–0.88)	0.111 (0.103– 0.119)	0.55 (0.44–0.64)	0.92 (0.87–0.96)
PZ	DCE-MRI	6 (8)	0.80 (0.77–0.82)	0.045 (0.028–0.065)	0.69 (0.47–0.87)	0.76 (0.67–0.83)
Visual	DCE-MRI	5 (6)	0.84 (0.79–0.87)	0.084 (0.071–0.097)	0.56 (0.38–0.73)	0.86 (0.79–0.92)
Nonvisual	DCE-MRI	11 (19)	0.82 (0.78–0.84)	0.071 (0.064–0.078)	0.54 (0.41–0.67)	0.84 (0.78–0.89)

Note—DCE-MRI = dynamic contrast-enhanced MRI, DWI = diffusion-weighted MRI, MRS = MR spectroscopy, TRUS = transrectal ultrasound, ECE = extracapsular extension, PZ = peripheral zone, TZ = transition zone.